JOURNAL OF APPLIED ELECTROCHEMISTRY **28** (1998) 1291–1297

Cathodic behaviour of RuO_2-doped Ni/Co_3O_4 electrodes in alkaline solutions: hydrogen evolution*

N. KRSTAJIC[‡], S. TRASATTI[§]

Department of Physical Chemistry and Electrochemistry, University of Milan, Via Venezian 21, 20133 Milan, Italy

Received 19 May 1997; revised 30 October 1997

RuO_2-doped Co_3O_4 electrodes were prepared by thermal decomposition of the corresponding nitrates using Ni as a support. The RuO_2 content was varied between 0 and 20 mol %. The kinetics of hydrogen evolution from alkaline solution was studied by recording quasisteady state polarization curves at several NaOH concentrations. A mechanism is proposed on the basis of Tafel slopes and reaction orders. The electrocatalytic activity of the mixed oxides has been found to go through a maximum at intermediate RuO_2 contents. Some evidence of instability has emerged.

Keywords: *electrocatalysis*, *hydrogen evolution*, *mixed oxide electrodes*, *Co_3O_4*, *RuO_2*, *reaction mechanism*

1. Introduction

Giuseppe Bianchi was actively involved in the development of oxide electrodes for technological applications [1–6]. Tests of materials for DSA® were already in progress in his laboratory during the early 1960s. It was in 1967 that he suggested a systematic study of the fundamental properties of RuO_2 and RuO_2-based electrodes [7]. This marked the beginning of the work of the present author in the area of electrocatalytic oxide electrodes. In this context, it is very appropriate to remember Giuseppe Bianchi by dedicating to his memory a paper on such electrode materials.

One of the targets of research in the field of oxide electrodes [8] is the replacement of expensive compounds with cheaper ones, or at least the development of systems able to reduce capital costs. In this context, in a previous paper [9], we have studied the surface behaviour of RuO_2-doped Ni/Co_3O_4 electrodes for cathode applications in alkaline solutions. It turns out that less than 10 mol % RuO_2 in a Co_3O_4 matrix is sufficient to attain the same surface response as pure RuO_2. In the previous paper the properties of mixed $RuO_2 + Co_3O_4$ electrodes were investigated by SEM, XPS and cyclic voltammetry in the composition range 0 to 20 mol % RuO_2. In this paper, we report results concerning the kinetics, mechanism and electrocatalysis of hydrogen evolution from alkaline solutions on the same set of electrodes used in the previous work.

2. Experimental details

Electrodes were prepared by thermal decomposition of appropriate mixtures of Co and Ru nitrate on a Ni support at 400 °C. Details of the preparation procedure have been given in the previous paper [9]. The oxide loading was on average 2 mg cm^{-2}. Electrodes were prepared with the following RuO_2 content: 0, 1, 2, 3, 5, 7.5, 10, 15, 20, 100 mol %.

Hydrogen evolution was studied in 1 mol dm^{-3} NaOH prepared with Milli-Q water. Reaction orders were determined by varying the NaOH concentration between 0.1 and 1.0 mol dm^{-3} keeping the ionic strength constant with $NaClO_4$. The measured pH of the solutions was 12.9, 13.2, 13.3, 13.5, 13.8 for 0.1, 0.2, 0.3, 0.5 and 1.0 mol dm^{-3} NaOH, respectively.

The Teflon holder for the electrodes and the three-compartment cell have been described previously [10]. Solutions were deaerated with purified nitrogen. Potentials were read and are reported against a saturated calomel electrode (SCE). Electrochemical measurements were carried out by means of Amel instrumentation (model 553 potentiostat, model 568 programmable function generator, and model 863 XY-recorder).

Quasisteady state polarization curves were recorded by first holding the electrode at −150 mV vs SCE for 10 min (this is close to the open-circuit potential), then at −1.0 V for 5 min and stepping the potential by 10 mV and reading the current after 1 min up to a potential were the current was of the order of 200 mA. The direction of potential variation was then reversed and the run continued until the current became anodic. For the determination of the reaction order complete polarization curves were recorded at each NaOH concentration following the procedure described above.

* This paper is dedicated to the memory of Professor Giuseppe Bianchi.
‡ Present address: Institute of Electrochemistry, University of Belgrade, Yugoslavia.
§ Author to whom correspondence may be addressed.

0021-891X

3. Results and discussion

3.1. *Polarization curves*

The first run of the polarization curves shows a marked hysteresis, irrespective of composition. In the second run the hysteresis disappears, as evident in Fig. 1. Hysteresis has been observed both with pure Co_3O_4 [11] as well as pure RuO_2 [12], although the origins are different. In both cases, the surface turns out to be 'prepared' to hydrogen evolution by some sort of reduction and/or site rearrangement. Since hydrogen is evolved on a modified surface, significant kinetic data are only those taken in the backward direction of potential variation. Furthermore, to attain more stable surface conditions, the whole kinetic analysis has been carried out on the data recorded in the backward direction during the second run.

All polarization curves show deviations from a Tafel line at higher current densities. There are, as a rule, related to uncompensated ohmic drops, but they can also imply a change in Tafel slope. Uncompensated ohmic drops include electrode, as well as electrolyte, resistance. The latter tends to increase with increasing current density due to the presence of gas bubbles in the electrolyte. Furthermore, the eventual presence of a film of gas bubbles on the electrode surface reduces the effective surface area. Both effects converge to increase deviations from the actual Tafel line with increasing overpotential.

With the aim of distinguishing between ohmic effects and change in Tafel slope, the experimental data were treated by assuming that the electrode potential, at each current, is given by the equation:

$$E = a + b \ln I + RI \tag{1}$$

where a and b are Tafel constant and slope, respectively, and R is the uncompensated resistance. In Equation 8 R is assumed to be a constant independent of current. The implications of such an assumption will be discussed later. Differentiating with respect to current:

$$\frac{dE}{dI} = \frac{b}{I} + R \tag{2}$$

Thus, plotting $\Delta E/\Delta I$ (where ΔE is the potential variation between two consecutive experimental points and ΔI is the related current variation) against $1/I$ should result in a straight line whose slope is b and whose intercept is R. The value of $1/I$ was taken in the middle of the ΔI interval. The resulting R was then used to correct the experimental polarization curve.

Figure 2 shows a typical analysis of the kinetic data. In Fig. 2(a) it is evident that two Tafel lines are hidden in the nonlinear sections of the polarization curves at high current densities (cf. Fig. 1). Figure 2(b) shows the experimental data when corrected using the value of R extrapolated from Fig. 2(a).

In the case of single Tafel slope and of a value of R increasing with current density, the plot in Fig. 2(a) would show an increase in $\Delta E/\Delta I$ for $I^{-1} \to 0$. Therefore, the observed shape of the plot can only be attributed to a change in Tafel slope to a higher value with increasing current density.

Figure 2(b) shows that subtraction of IR values from the experimental potential, E, results in a reasonably linear plot showing a modest deviation from the theoretical value of 120 mV. Thus, R turns out to be under- rather than overestimated as would be the case if it increased markedly with current as a consequence of bubble effects. R values may be quantitatively in error up to 20%.

Figure 3 gathers the polarization curves for a number of compositions, after correction for uncompensated IR drops. Two aspects are worthy of comment: (i) the overpotential decreases as the RuO_2 content increases, and (ii) a single Tafel line with slope close to 120 mV decade^{-1} is observed for electrodes with composition close to Co_3O_4, while a second Tafel line of slope close to 40 mV decade^{-1} appears at lower current densities as the RuO_2 content increases.

The results of the kinetic analysis are summarized in Table 1. It is not possible to rule out the presence of two Tafel lines at all compositions (with the exception, perhaps, of pure Co_3O_4). At certain compositions the second Tafel line probably falls outside the explored current density range which is 0.01 to 100 mA cm^{-2} here. It is in fact interesting to note that the current where the break in the Tafel line is observed, is a function of the oxide composition. This is also shown in Table 1.

The uncompensated resistance, R, derived from the treatment of the kinetic data, is summarized in Table 1. The value of R is relatively small at all compositions, increasing slightly as the RuO_2 content increases. R encompasses the solution resistance (at the Luggin capillary), as well as any ohmic drops across the oxide layer. The latter includes any contact resistance between the oxide overlayer and the Ni

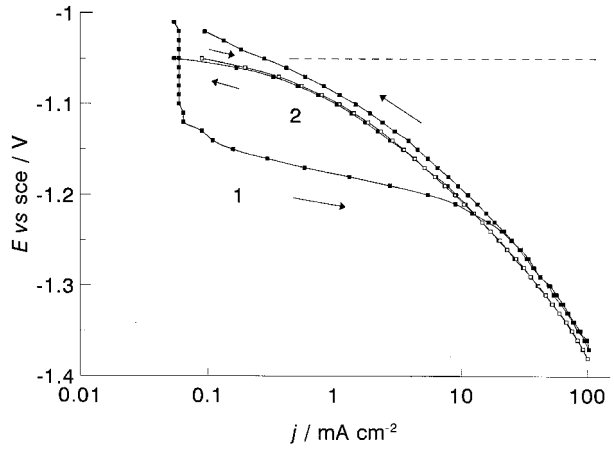

Fig. 1. Potential versus current density curves for hydrogen evolution from 1 mol dm^{-3} NaOH on a Co_3O_4 electrode with 5 mol % RuO_2. (1) First run; (2) second run. Arrows indicate the direction of potential variation. (- - - -) Position of the reversible potential for the H_2 reaction.

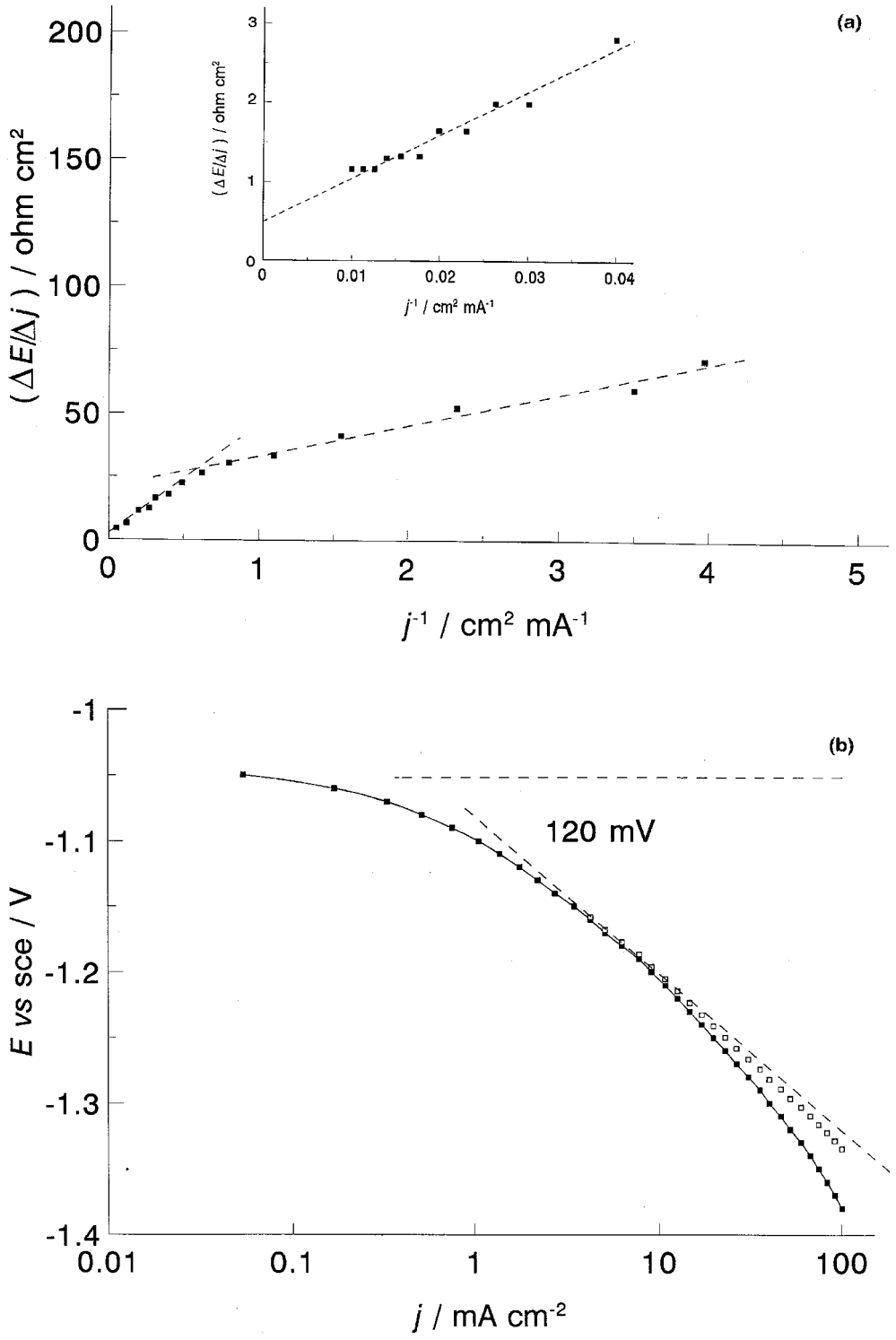

Fig. 2. (a) Application of Equation 2 in the text to the current–potential data (2nd run, reverse direction) of Fig. 1 to derive ohmic drop and Tafel slopes. Inset: enlargement of the initial part of the main plot to give evidence to the intercept. (b) Experimental data (■) corrected for *IR* drop (□). (- - - -) Theoretical Tafel slope.

support. Although separation of the various components is impossible, it should be noted that the observed *R* values are of the same order of magnitude as those usually measured at metal electrodes and are attributable to the electrolyte resistance. If insulating layers were present between the active oxide and the support, these would have resulted in much higher *R* values. The small average value of *R* indicates that no compact NiO has grown between the support and the active layer in the course of preparation. The slightly higher value of *R* at high RuO_2 contents may be a consequence of a poorer miscibility of NiO and RuO_2.

The introduction of a small amount of RuO_2 to a mixture with Co_3O_4 modifies both the electrocatalytic properties and the hydrogen evolution mechanism. Figure 4 shows the dependence of the potential at 100 mA cm^{-2} (after *IR* correction) on the RuO_2 con-

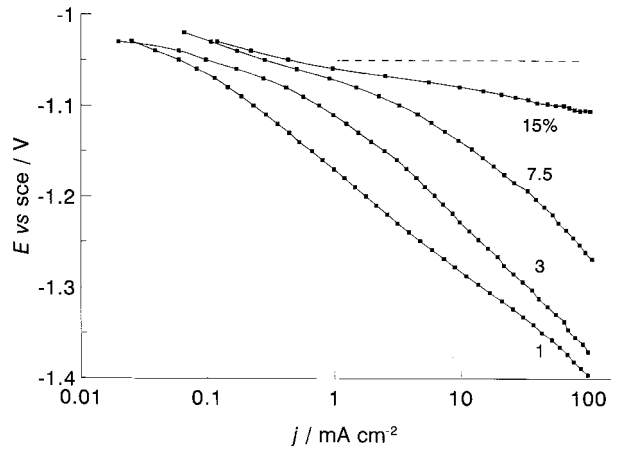

Fig. 3. Tafel plots in 1 mol dm^{-3} NaOH corrected for *IR* drop. The content of RuO_2 in the mixture is indicated. (- - - -) Position of the reversible potential for the H_2 reaction.

tent. There is a jump of more than 0.2 V between 5 and 10% RuO_2. At higher RuO_2 contents the overpotential does not change appreciably. With reference to the XPS data reported in the previous paper [9], the increase in activity occurs in the very composition range where a dramatic surface enrichment with RuO_2 takes place. The observed decrease in overpotential may be related to a change in mechanism as Ru replaces surfaces Co sites.

Figure 4 also shows that the overpotential for 100% RuO_2 is higher than that for 20% RuO_2 despite the fact that the surface of the mixed oxide is saturated with RuO_2 and should thus behave as pure RuO_2. A reason for this may be the higher surface area (as measured by the voltammetric charge) of 20% RuO_2, as shown in the previous work [9], which contributes to reduced overpotential. However, synergetic effects in RuO_2 + Co_3O_4 mixtures cannot be ruled out. In fact, the Tafel slope is lower for RuO_2-rich mixtures than for pure RuO_2, which points to a mechanistic change.

Table 1. Kinetic parameters for hydrogen evolution on Co_3O_4 + RuO_2 electrodes

RuO_2 /mol %	b^1 /mV decade^{-1}		R^2 /Ω	$j_x{}^3$ /mA cm^{-2}
0	105		0.13	–
1	115		0.18	–
2	42	125	0.16	1
3	45	128	0.12	1.2
5	42	125	0.24	2.2
7.5	41	122	0.20	4.5
10	38		0.45	–
15	31		0.55	–
20	27		0.43	–
100	41		0.35	–

[1] Tafel slope, eventually at low and high overpotentials.
[2] Uncompensated resistance, derived from the intercept of plots like that in Fig. 2(a).
[3] Value of current density at the transition point between two Tafel slopes.

3.2. *Reaction order*

Figure 5 shows complete sets of polarization curves at different pH values for two oxide compositions. The Tafel slope does not depend on solution pH. At low RuO_2 content a single Tafel slope of about 120 mV decade^{-1} is found, whereas at high RuO_2 contents the Tafel slope is close to 30 mV decade^{-1}. At intermediate compositions two Tafel lines are possibly present. However, the composition range where two Tafel lines are present was observed to shift slightly to higher RuO_2 content with prolonged use of the electrodes. It is as though the surface activity of RuO_2 decreased.

The above phenomenon is particularly evident in Fig. 4. In fact, the curve of the dependence of overpotential on the mixed oxide composition is shifted to higher RuO_2 content on aged electrodes. In view of the strong surface enrichment with RuO_2, such an effect can only be understood in terms of a decrease in RuO_2 surface concentration, which is understandably more evident at intermediate surface enrichment.

Reasons for such depletion in RuO_2 may be several. However, the most plausible ones are: (i) During prolonged hydrogen evolution some surface layers are mechanically removed with exposure of regions with less RuO_2; (ii) RuO_2 dissolves in alkaline solution during anodic potential scans to determine the surface voltammetric charge. The latter reason is less probable since the anodic limit of the voltammetric curves is below the critical potential for RuO_2 dissolution [13]. On the other hand, erosion of the Co_3O_4 surface during hydrogen evolution has been detected in previous work [11]. Thus, these data point to an intrinsic instability of the electrodes. Although the rate of erosion may be very small, the consequence on the electrode performance may be dramatic in view of the correlation between activity and RuO_2 surface concentration.

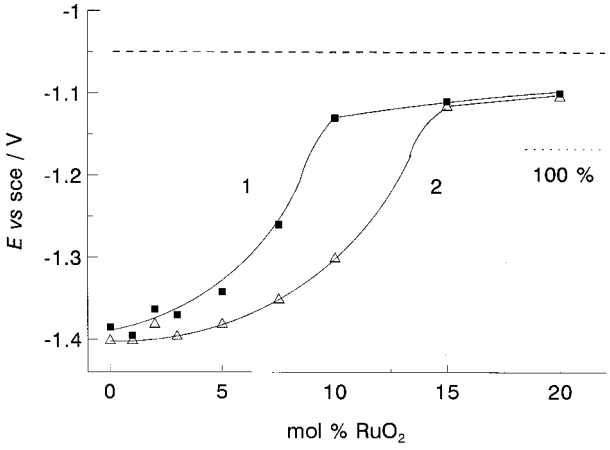

Fig. 4. Dependence of the electrode potential for hydrogen evolution at 100 mA cm^{-2} on the electrode composition. (1) Initial value; (2) value recorded after the whole kinetic study. (- - - -) Position of the reversible potential for the H_2 reaction (1 mol dm^{-3} NaOH). The value of the potential for pure RuO_2 is also indicated.

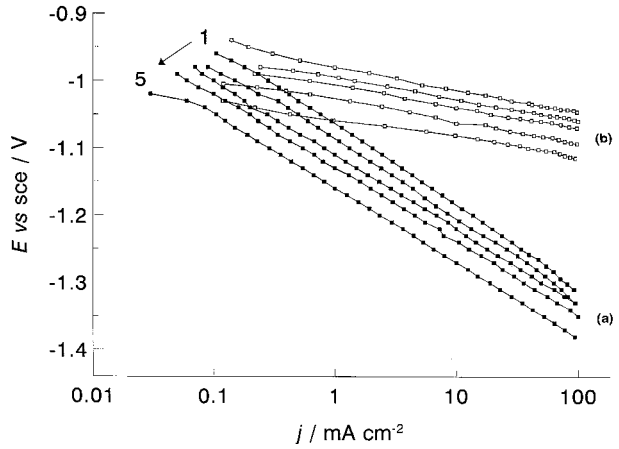

Fig. 5. *IR*-corrected Tafel plots for hydrogen evolution at various pH. (1) 12.9; (2) 13.2; (3) 13.3; (4) 13.5; (5) 13.8. (a) 2 mol % RuO_2; (b) 15 mol % RuO_2.

Figure 6 shows representative kinetic data as a function of pH. For pure Co_3O_4 (Tafel slope close to 120 mV decade^{-1}), the observed reaction order is about -0.5. For 10% RuO_2, the reaction order in the potential range of the higher Tafel slope is again close to -0.5, whereas in the low Tafel slope region it is close to -1.5. Finally, for 20% RuO_2 for which is single Tafel slope of 30 mV is observed, the reaction order is close to -2.

3.3. *Reaction mechanism*

A general mechanism is proposed. The Tafel slope of 120 mV decade^{-1} is indicative of a slow primary discharge step:

$$H_2O + S{-}OH + e^- \rightarrow S\begin{matrix}H\\ \diagup\\ \diagdown\\ OH\end{matrix} + OH^- \qquad (2a)$$

where S—OH is a surface site. In alkaline solution the discharging particles are water molecules. Thus, if step (2a) is rate determining, the reaction order should be zero with respect to OH^- concentration.

The observed reaction order of -0.5 can be understood in terms of surface acid–base equilibria [14]. The oxide surface is covered by OH groups which undergo dissociation in solution with charging of the oxide surface [15]. In alkaline solution:

$$S{-}OH + OH^- \rightarrow S{-}O^- + H_2O \qquad (3)$$

The surface charge gives rise to an interfacial potential. Although the reaction order is determined at constant ionic strength, the surface charge changes with pH even at constant potential. Thus,

$$\phi^* = \frac{-RT}{F}\ln[OH^-] \qquad (4)$$

where ϕ^* is the electric potential at the reaction site. For Reaction 2a, in the presence of a variable interfacial potential:

$$j \propto \exp\left[\frac{-\alpha(E-\phi^*)F}{RT}\right] \qquad (5)$$

From Equations 4 and 5:

$$\ln j \propto \left[\frac{-\alpha EF}{RT}\right] - \alpha \ln [OH^-] \qquad (6)$$

According to the definition of reaction order (at constant potential) [16]:

$$\beta_{OH^-} = \frac{\mathrm{d}\ln}{\mathrm{d}\ln[OH^-]} = -\alpha \qquad (7)$$

Equation 7 shows that the acid–base properties of an oxide surface can produce fractional reaction orders. Similar observations have been made with other oxides for both hydrogen [12] and oxygen evolution [14].

Along the same lines, a reaction order close to -1.5 with a 40 mV decade^{-1} Tafel slope indicates that the mechanism is limited by a second electron transfer on an oxide surface giving rise to pH-dependent surface charging. For instance, the step following step (2a) can be

$$S\begin{matrix}H\\ \diagup\\ \diagdown\\ OH\end{matrix} + e^- \rightarrow S{-}H + OH^- \qquad (2b)$$

Such a step would correspond to complete reduction of the surface active site (although this does not imply destruction of the oxide structure).

With step (2b) rate determining and step (2a) close to equilibrium, the rate equation is (assuming a very small coverage with H):

$$j \propto \left[\frac{-(1+\alpha)EF}{RT}\right] - (1+\alpha)\ln [OH^-] \qquad (8)$$

The reaction order is thus

$$\beta_{OH^-} = \frac{\mathrm{d}\ln}{\mathrm{d}\ln [OH^-]} = -(1+\alpha) \qquad (9)$$

that is, -1.5 with $\alpha = 0.5$.

Finally, the reaction order close to -2 with a Tafel slope of about 30 mV decade^{-1} can be explained by a

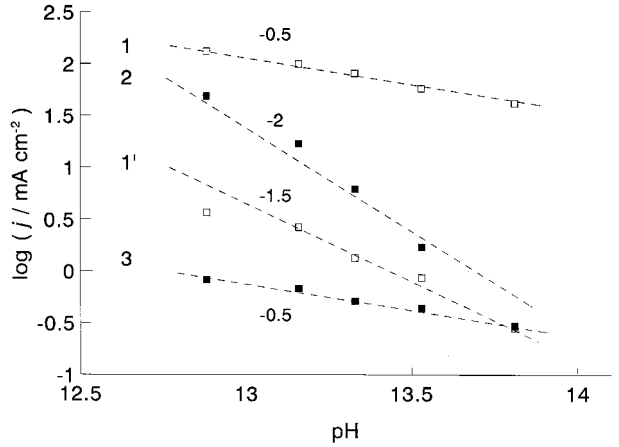

Fig. 6. Current–pH plots for the determination of reaction orders with respect to OH^-. RuO_2 content: (1, 1′) 10 mol %; (2) 20 mol %; (3) pure Co_3O_4. Electrode potential: (1) -1.25 v; (1′) -1.05 v; (2) -1.025 v; (3) -1.1 v *vs* SCE. (- - - -) Theoretical slopes (indicated by the lines).

chemical step following the two consecutive electron transfer steps (an EEC mechanism). For instance,

$$S{-}H + H_2O \rightarrow S{-}OH + H_2 \qquad (2c)$$

In this case it is easy to show that the surface acid–base equilibria do not result in fractional reaction orders.

The second Tafel slope of 120 mV decade^{-1} with step (2b) being rate determining can be interpreted (i) as a transition from $\theta_H \approx 0$ to $\theta_H \approx 1$. This would imply that the active sites are always Ru atoms. Since as step (2a) is rate determining the active sites are presumably Co atoms, it cannot be ruled out that (ii) the transition from 40 to 120 mV Tafel slope marks the difference between two types of active sites. In view of the poorer activity of Co sites [12], however, an intermediate Tafel slope would be more plausible. The second Tafel slope could also be due to (iii) transition from step (2b) to step (2a) as rate determining on the same Ru sites.

3.4. *Electrocatalysis*

The increase in activity from pure Co_3O_4 to 10–20% RuO_2 in Fig. 4 corresponds to about two orders of magnitude in terms of reaction rate. In principle, electronic effects should be separated from geometric effects to detect true electrocatalytic effects. In this work this is not possible. Although the voltammetric charge, q^*, is usually used as a measure of the electrochemically active surface area [8], after prolonged hydrogen evolution q^* turns out to be much higher than for fresh electrodes because of the Co_3O_4 matrix reduction [11]. Thus, the differences in surface area are concealed by the large q^* variation related to the matrix.

The above argument is illustrated by Fig. 7 where the voltammetric charge for fresh electrodes is plotted against the charge determined after the polarization curves. It is evident that the charge is up to two orders of magnitude higher after polarization. This charge can no longer related to surface sites only, but it includes also redox transition in the bulk of the Co_3O_4 matrix; therefore, it cannot be used to normalize the experimental current density.

Since the initial charge for 10–20% RuO_2 electrodes is about only twice that for 1% RuO_2, the much higher activity ratio cannot be related only to surface area effects. On the other hand, q^* includes Ru and Co sites while hydrogen evolution takes place mostly on Ru sites. Thus, the increase in activity is associated with the surface concentration of RuO_2. Although one surface Ru site is (to a first approximation) equivalent to one surface Co site in terms of q^*, this is not the case in terms of electrocatalytic activity. In this context, the plot in Fig. 4 can be rationalized by using the surface concentration of Ru [9] rather than the bulk composition. Figure 8 shows that a linear correlation exists between log j and the *surface* concentration of Ru sites. The fact that the reaction rate is not simply proportional to the surface concentration of Ru atoms implies that the major factor in the electrocatalytic enhancement of these electrodes is the decrease in Tafel slope with increasing RuO_2 content, that is, a typical electronic effect.

On the other hand, the slightly higher overpotential of pure RuO_2 with respect to the saturation value in Fig. 4 can be explained in terms of surface area effects, since the surface composition is always 100% RuO_2. In fact, the surface charge for pure RuO_2 for fresh electrodes is somewhat lower than that for 20% RuO_2 by almost the same ratio as the electrocatalytic activity [9].

4. Conclusions

(i) Doping Co_3O_4 with RuO_2 increases the electrocatalytic activity for hydrogen evolution in alkaline solutions by about two orders of magnitude as the doping content is only 10 mol % RuO_2. In this composition range the surface of the mixed oxides is dramatically enriched with Ru.

(ii) The introduction of RuO_2 in a Co_3O_4 matrix changes the mechanism of hydrogen evolution;

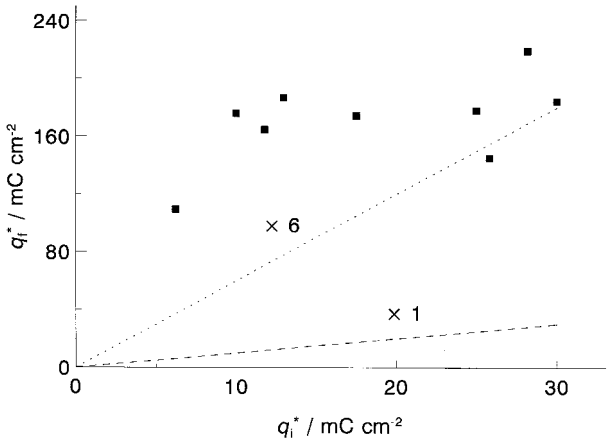

Fig. 7. Plot of the voltammetric charge in 1 mol dm^{-3} NaOH for fresh electrodes against the voltammetric charge at the end of the whole kinetic study. The figures by the lines indicate their slope.

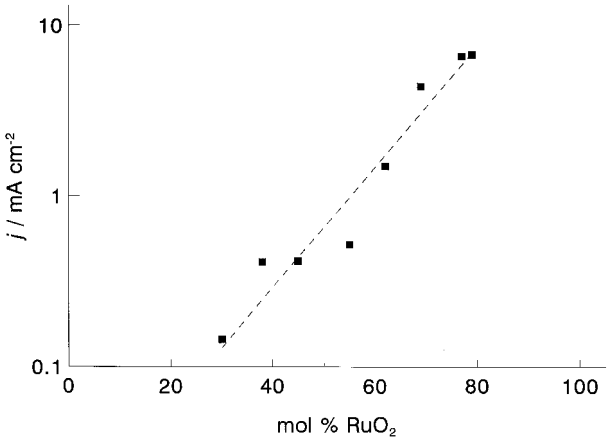

Fig. 8. Semilog plot of current for H_2 evolution in 1 mol dm^{-3} NaOH at $E = -1.08$ V *vs* SCE (from data in Fig. 3) as a function of the surface RuO_2 concentration [9].

the Tafel slope changes from 120 mV decade^{-1} at low RuO_2 content to 30 mV decade^{-1} at high RuO_2 concentrations passing through a composition range where the two Tafel slopes are simultaneously present.

(iii) Fractional reaction orders with respect to OH^- are observed. These can be interpreted in terms of double layer effects related to the pH-dependent surface charging mechanism of oxides in aqueous solution.

(iv) Prolonged hydrogen evolution shifts the transition region described above to higher RuO_2 contents. This is indicative of surface RuO_2 depletion, presumably related to mechanical erosion phenomena. Thus, these oxide mixtures, electrocatalytically interesting for the small amount of RuO_2 necessary to attain higher activities than pure RuO_2, show stability problems which need to be studied in greater detail.

Acknowledgements

N.K. thanks the ECC (Brussels) for a research fellowship (1992). This work was supported by ECC and CNR (Rome).

References

[1] G. Bianchi, V. De Nora, P. Gallone and A. Nidola, *US Patent Appl. 778 736* (1968).
[2] G. Bianchi and A. Nidola, *US Patent 3 428 544* (1969).
[3] G. Bianchi, P. Gallone and A. Nidola, *US Patent 3 491 014* (1970).
[4] O. De Nora, A. Nidola, G. Trisoglio and G. Bianchi, *British Patent 1 399 576* (1973).
[5] G. Bianchi, V. De Nora, P. Gallone and A. Nidola, *US Patent 3 948 751* (1976).
[6] G. Bianchi, *J. Appl. Electrochem.* **1** (1971) 231.
[7] S. Trasatti and G. Buzzanca, *J. Electroanal. Chem.* **29** (1971) App. 1.
[8] S. Trasatti, in 'The Electrochemistry of Novel Materials', edited by J. Lipkowski and P. N. Ross (VCH, Weinheim, 1994), p. 207.
[9] N. Krstajic and S. Trasatti, *J. Electrochem. Soc.* **142** (1995) 2675.
[10] R. Garavaglia, C. M. Mari and S. Trasatti, *Surf. Technol.* **23** (1984) 41.
[11] E. Veggetti, I. M. Kodintsev and S. Trasatti, *J. Electroanal. Chem.* **339** (1992) 255.
[12] S. Trasatti, in 'Modern Chlor-Alkali Technology', edited by T. C. Wellington (Elsevier Applied Science, Amsterdam, 1992), p. 281.
[13] R. U. Bondar and E. A. Kalinovskii, *Elektrokhimiya* **14** (1978) 730.
[14] C. Angelinetta, M. Falciola and S. Trasatti, *J. Electroanal. Chem.* **205** (1986) 347.
[15] A. Daghetti, G. Lodi and S. Trasatti, *Mater. Chem. Phys.* **8** (1983) 1.
[16] B. E. Conway and M. Salomon, *Electrochim. Acta* **9** (1964) 1599.